Thermal and Vibration Characterization of Flexible Heat Sinks

by

Saurabh Shirish Prabhu

A Dissertation Presented in Partial Fulfilment
of the Requirements for the Degree
Master of Science

Approved June 2019 by the
Graduate Supervisory Committee:

Konrad Rykaczewski, Chair
Patrick Phelan
Robert Wang

ARIZONA STATE UNIVERSITY

August 2019

ABSTRACT

In nature, it is commonly observed that animals and birds perform movement-based thermoregulation activities to regulate their body temperatures. For example, flapping of elephant ears or plumage fluffing in birds. Taking inspiration from the nature and to explore the possibilities of such heat transfer enhancements, augmentation of heat transfer rates induced by the vibration of solid and well as novel flexible pinned heatsinks were studied in this research project. Enhancement of natural convection has always been very important in improving the performance of the cooling mechanisms. In this research, flexible heatsinks were developed and they were characterized based on natural convection cooling with moderately vibrating conditions. Vibration of heated surfaces such as motor surfaces, condenser surfaces, robotic arms and exoskeletons led to the motivation of development of heat sinks having flexible fins with an improved heat transfer capacity. The performance of an inflexible, solid copper pin fin heat sink was considered as the baseline, current industry standard for the thermal performance. It is expected to obtain maximum convective heat transfer at the resonance frequency of the flexible pin fins. Current experimental results with fixed input frequency and varying amplitudes indicate that the vibration provides a moderate improvement in convective heat transfer, however, flexibility of fins had negligible effects.

DEDICATION

This dissertation is dedicated to Aai, Baba and Sayali for supporting me throughout this journey and helping me become what I am today.

ACKNOWLEDGMENTS

I would thank Dr. Konrad Rykaczewski for his guidance and teaching me good morals and research ethics. I am honoured and grateful that Dr. Patrick Phelan and Dr. Robert Wang agreed to be a part of my thesis committee. Dr. Matthew Ralphs played an important role by believing in me and giving me an opportunity to work with him. I would thank Dr. Bruce Steele for letting us use wind tunnel during the initial phase of this project. I would like to express my gratitude towards Rykaczewski Research Group especially Praveen Kotagama, Dr. Akshay Phadnis, Chad Manning and Wilson Kong for their invaluable feedbacks and support. Working with Rykaczewski Research Group was the best learning experience. I would also thank my school friends Ninad Joshi and Digvijay Adsare for helping me get access to the research papers and books that I could not access. I would thank all my colleagues at the Parking and Transit Services for their assistance during the critical times. I am grateful to my roommates, Swapneel Danayat, Sangeet Sankarmangalam Ulhas and Akshay Nair, all the friends at ASU who became my family, family back home, everyone at dad's office and all those who helped me directly or indirectly during each and every step of my journey here as a graduate student.

TABLE OF CONTENTS

Page

CHAPTER Page

LIST OF TABLES

Table Page

LIST OF FIGURES

Figure Page

Figure Page

NOMENCLATURE

Symbol	Definition
δ	Logarithmic Decrement
t	Time (s)
$x(t)$	Position of the pin at time t (m)
T_d	Period of oscillation (s)
A	Amplitude of vibration (m)
A_x	Area of region x (m^2)
ζ	Dimensionless damping ratio
ω_n	Natural Frequency (rad/s)
ω_d	Damped natural frequency (rad/s)
ϕ	Phase difference (rad)
K_r	Rotational stiffness (N/m)
K_t	Translational stiffness (N/m)
L	Length (m)
E	Youngs Modulus (N/m^2)
I	Moment of inertia (m^4)
m	Mass per unit length (Kg/m)
y	Deflection of the cantilever beam along y axis (m)
f_n	Natural frequency (Hz)
L_c	Characteristic Length (m)
h	Convective Heat transfer coefficient (W/m^2K)
K	Conductivity of the material (W/m-K)
Nu	Nusselt Number $\frac{hL_c}{K}$

Symbol	Definition
Ra	Rayleigh Number $\frac{g\beta(T_s-T_{air})L_c^3}{\nu\alpha}$
Re	Reynolds Number $\frac{VL_c}{\nu}$
Gr	Grashofs Number $\frac{g\beta(T_s-T_{air})L_c^3}{\nu^2}$
V	Velocity (m/s)
Q	Heat Transfer (W)
T_s	Surface Temperature (K)
T_{air}	Ambient air Temperature (K)
ϵ	Approximate Emissivity of the material
σ	Stefan-Boltzmann constant (W/m^2K^4)
g	Gravitational Acceleration 9.80665 (m/s^2)
β	Coefficient of volume expansion $\frac{1}{T}$ (1/K)
Pr	Prandtl Number
ν	Kinematic Viscosity of the fluid (m^2/s)
α	Thermal Diffusivity (m^2/s)
S_h	Horizontal spacing between the two pin fins (m)
S_v	Vertical spacing between the two pin fins (m)
ρ	Density of the fluid (kg/m^3)
η	Efficiency
F_d	Damped Natural Frequency (Hz)
F_n	Undamped Natural Frequency (Hz)
$T\#$	Thermocouple Number
RHr	Resistance Heater
$PDMS$	Polydimethylsiloxane

Symbol	Definition
TIM	Thermal Interface Material
LM	Liquid Metal (Galinstan)
OEM	Original Equipment Manufacturer
AC	Alternating Current (A)
fps	Frames per second (f/s)
RGB	Red-Green-Blue format
ROI	Region of interest
$MEMS$	Micro Electro Mechanical Systems

CHAPTER 1

Introduction

Enhancement of natural convection has been very important in improving the performance of the cooling mechanisms of various devices.[1]–[3] Research on various geometries and materials have led to today's most optimised design of metal heatsinks that are used in electronics.[4]–[15] Many researchers have studied the effects of vibrations on the overall heat transfer in the cooling mechanisms. [1], [2], [15]–[27]

Li et. al. developed a self-agitator for convective heat transfer enhancement by taking an inspiration from a wind induced vibrations of the grass blades.[19] Vast research is already been done on vibrating heat exchangers and it is safe to say that vibration induced heated surface could enhance heat transfer rates.[26][18] Though vibration in any rotating/moving instrument is considered as the inimical factor for causing damage, L. Cheng et. al. argued that the vibrations of the surfaces could enhance heat transfer in the heat exchangers.[26] Selimenfendigil et. al. provided a very important finding from their project that would play a very important role in this report; they showed that as the Youngs modulus of surface material decreases, the averaged Nusselt number increases thus improving the heat transfer by 66%.[28] Prstic et. al. studied the effects of airflow over a heatsink inside an air duct and found that the flow bypass increases with increasing fin density and clearance and is found to be relatively insensitive to inlet duct velocity.[29] Flexible heat spreaders and heat sink sheets have been in use for over a decade. [22] The heat transfer rate through the thermal boundary layer increases when the hot surface is induced with vibrations.[22][24] At higher rates of vibrations the thermal boundary layer starts getting unstable. Fu et. al confirmed that higher the vibration of the wall, the greater the heat transfer rate. [30] Alben et. al.

claimed a 60% improvement in heat transfer rates when the air induced Poiseuille flow inside the channel becomes unstable. [31] Crittenden et al., Rips et al., Shoele and Mittal showed that forced convection can make the flexible fins vibrate and move, thus increasing the heat transfer by increasing turbulence and disturbing the thermal boundary layer. [8], [15], [32]

Lee et. al. claimed that flexible flags clamped vertically in a channel flow could increase the heat transfer.[17][25] The use of vibrating reeds to induce vortex shedding with low pressure losses could improve heat transfer performance. [8][17][25] Similarly, Park et. al. investigated a self-oscillating inverted flag and its effect on the enhancement in heat transfer; they found an increase in efficiency by a factor of 1.2.[27] Rips et. al. studied a novel method that exploits flow-induced vibration for enhancing heat transfer in electronic cooling applications using coupled flow-structural-thermal modelling.[8] The self-actuated fluttering reeds leads to the extraction of unused momentum from the flow and mix the cold core fluid with the hot fluid near the walls.[8] Introduction of the reed into the heat channel leads to an increase in the heat transfer rate by 30% for a fixed flow rate.[8] Go et. al. investigated the feasibility of heat transfer enhancement by implementing flow induced vibration in a micro-fin array. They found 5.5% enhancement in cooling rates.[3] Jamesahar et. al. worked on the unsteady natural convective heat transfer of an incompressible fluid in a square cavity which was divided into two triangles with the help of a very thin flexible thermal conductive membrane. They found that final shape of a flexible membrane plays an important role and the heat transfer from a flexible membrane was higher than that of a rigid membrane.[33] Khanafer compared the flow and heat transfer characteristics in a lid-driven cavity between flexible and modified geometry of a heated bottom wall. He found a substantial enhancement in heat transfer of 61.4% in

the case of flexible bottom wall as compared to a flat bottom wall case at Grashof number of 10^4 and Reynolds number less than 400.[2] Kumar conceptualized a novel method to eliminate the external pumps in the heat exchangers by dynamically deforming one of the walls; this led to increase in heat transfer coefficient with increase in the amplitude of deformation of the wall.[34][21]

Toshio Aihara and Shigenao Maruyama carried out free convection and radiative experiments on dense pin fin arrays. They came up with correlations for calculating apparent emissivity an of the pin fin array and overall radiative heat transfer.[35]

Vibration of heated surfaces can increase the heat transfer rates thus reducing the surface temperatures. In this research, vibration of heated surfaces lead to the motivation of development of flexible type heat sinks with potentially improved heat transfer capacity. Parameters that affect the heat transfer rates in the flexible heatsinks are also investigated.

This report is divided into 6 chapters. Chapter 1 covers a brief introduction to the previous work done related to the effects of vibration and disturbance of thermal boundary layer on the overall heat transfer of the different surfaces and devices. Fabrication methods of the heatsinks and steps taken to tackle unsuccessful bonding of a polymer to a metal were discussed in chapter 2. Chapter 3 discusses the arrangement of the experimental setup and data collection methods. Analytical methods and different models were compared in chapter 4. Results and Discussions are covered in chapter 5. This report is concluded with conclusions and future scope in chapter 6.

CHAPTER 2

Fabrication Methods

Fabrication of Heat sinks

A 5 mm thick plate was cut into squares of $38 \times 38\ mm^2$. 3 holes were drilled through the 5 mm thick edge for possible thermocouple attachments. 121 number of 2.5 mm deep and 1.78 mm diameter holes were drilled along one of the $38 \times 38\ mm^2$ surfaces using a vertical milling machine to provide support to the individual pins. 1-inch long pins were cut out of a 1.5 mm diameter copper wire and the ends were polished flat using 600 grit polishing paper on the polishing machine.

PDMS (polydimethylsiloxane) also referred as silicones belong to the group organosilicones.[36] Silicones have a low toxicity, a low chemical reactivity and are thermally stable over a range of -100^oC to 250^oC. For fabrication of flexible pin fin joints, EcoFlex 00-30 with 50:50 ratios of part A and Part B were used. EcoFlex 00-30 is stable in the range of-65^oC to 232^oC and cures within 4 hours.[37]

A Plexiglass fixture was fabricated using laser cutting to keep pin fins positioned upright until EcoFlex 00-30 cures. Vacuum chamber was used to get rid of air bubbles before the EcoFlex 00-30 cures.

3 types of flexible heat sinks were fabricated having same dimensions as that of a baseline rigid heatsink[38] but different compositions of bonding material in between the pins and the copper base plate. First type consisted of the bonding material made of pure EcoFlex 00-30, second type had PDMS with Wakefield Type 120 Thermal interface material (TIM) [39] and third type consisted of bonding material made of EcoFlex 00-30 and 15% Galinstan by weight[40]. The geometries of all 3 flexible heat

sinks were replicas of an original equipment manufacturer(OEM) made copper heat sink by Enzotech CNB-S1 [38].

Table 1 Composition of the Heat Sinks

Heat sink	**Surface treatment**	**Silicone Composition**	**Manufacturer**
Rigid Heat sink	N/A	N/A	Enzotech CNB-SI
Flexible Heat sink 1	(3-Trimethoxysilylproply) Diethylenetriamine- Tech-95	EcoFlex 00-30	Self-Fabricated
Flexible Heat sink 2	(3-Trimethoxysilylproply) Diethylenetriamine- Tech-95	Wakefield Type 120 + EcoFlex 00-30	Self-Fabricated
Flexible Heat sink 3	(3-Trimethoxysilylproply) Diethylenetriamine- Tech-95	15% Galinstan in EcoFlex 00-30	Self-Fabricated

A typical fabrication process of the flexible heat sinks is shown in the figure below.

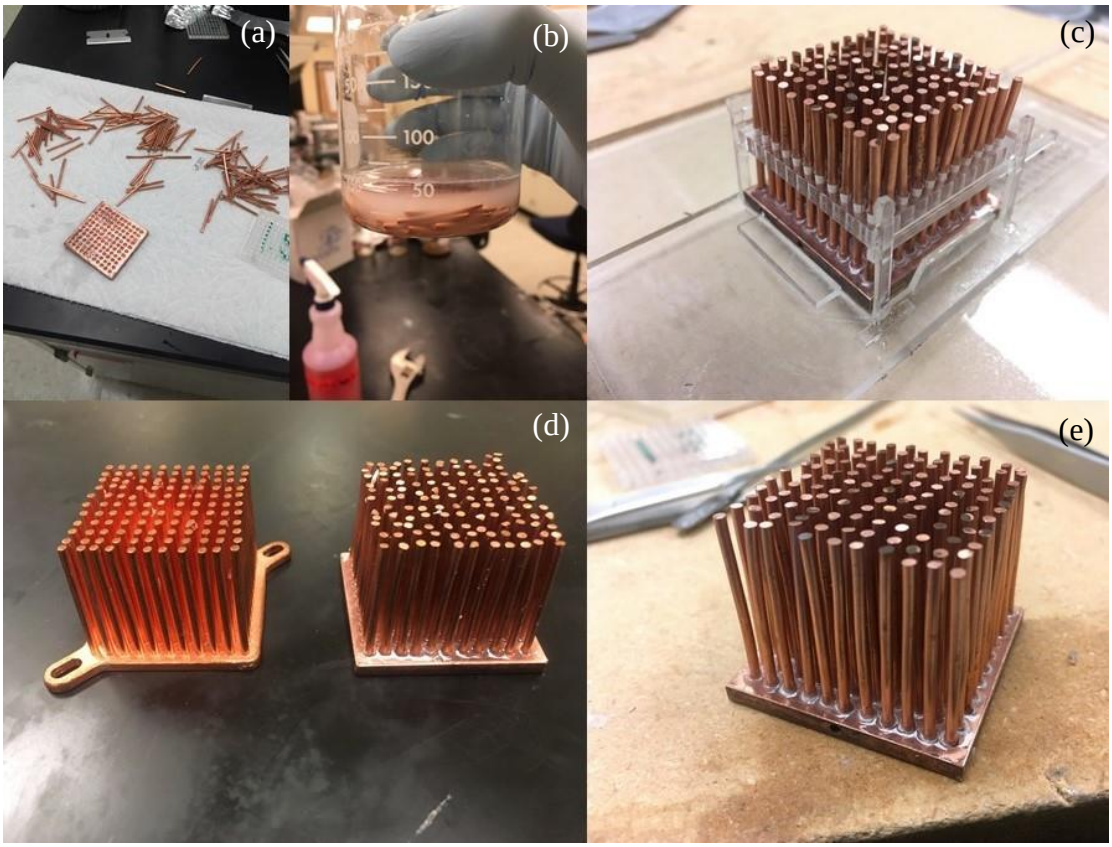

Figure 1(a) Copper Base plate and Pin fins (b) Treatment with (3-Trimethoxysilylproply) Diethylenetriamine- Tech-95 (c) Plexiglass fixture (d) Enzotech CNB S1 Rigid Heat Sink and Flexible Heat Sink 1 (e) final product (Flexible heat sink 2)

Figure 1 (a) shows the different parts of a typical flexible heatsink before assembly. All the parts were fabricated manually in the lab. The parts were washed in distilled water and ethanol and blow dried to get rid of oils and dust. Figure 1 (b) shows the treatment of all the parts with silane coupling agent called (3-Trimethoxysilylproply) Diethylenetriamine – Tech 95. Silane coupling agents are usually deposited through any alcohol; ethanol in this case.[41]. Once the surfaces were treated with silane coupling agent, they were allowed to dry and 1:1 Ecoflex 00-30

(and/or TIM or LM) was applied on the upper surface of the copper base plate. The pin fins were inserted in the holes using the Plexiglass fixture shown in the Figure 1(c) and the whole assembly was allowed to cure overnight. Once the Ecoflex 00-30 was cured, the fixture was removed, and the final product was obtained as shown in Figure 1(d). Figure 1(e) shows side by side comparison of the flexible heatsink and the standard OEM made Enzotech CNB S1 rigid heatsink.

Bonding of pin fins with the base plate was a very critical step in the overall fabrication process because the polymer bonds would fail if the metal surfaces were not treated with silane coupling agents. Moreover, excess use of silane coupling agents would cause EcoFlex 00-30 to form a thick slimy polymer layer which would never cure causing failed bonds. For a perfect consistency of the cured Ecoflex 00-30, the surface treatment process played a critical role. During the treatment, the concentration of the silane coupling agent in ethanol was kept below 2% and the temperature was fixed to 60^{o}C. The metal parts were kept in this chemical mixture for 20 to 30 mins. The working of the silane coupling agent is discussed in the following section

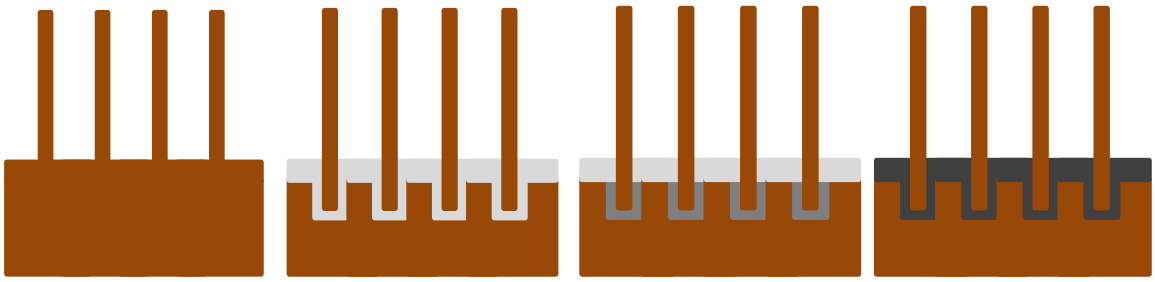

Baseline Heatsink
Enzotech CNB S1

Flexible Heatsink 1
EcoFlex 00-30

Flexible Heatsink 2
Wakefield type 120
& Ecoflex00- 30

Flexible Heatsink 3
Galinstan
+ EcoFlex 00-30

Figure 2 Different heatsinks and their bond compositions

Bonding of copper with silicone

Silane coupling agents are the group of silanes that promote adhesion or bonding between dissimilar materials i.e. bonding of organic polymers to inorganic substrates.[42]–[44] To form a strong, durable bond between copper surface and Silicone, a silane coupling agent was used. (3-Trimethoxysilylproply) Diethylenetriamine- Tech-95 [45] was used to form a silane layer on the copper surface through the process of hydrolysis with the help of ethanol at elevated temperatures of about $40^o - 50^oC$. This silane layer formed a strong bond with copper substrate and silicone. A typical working of a silane coupling agent is shown in the figure below.

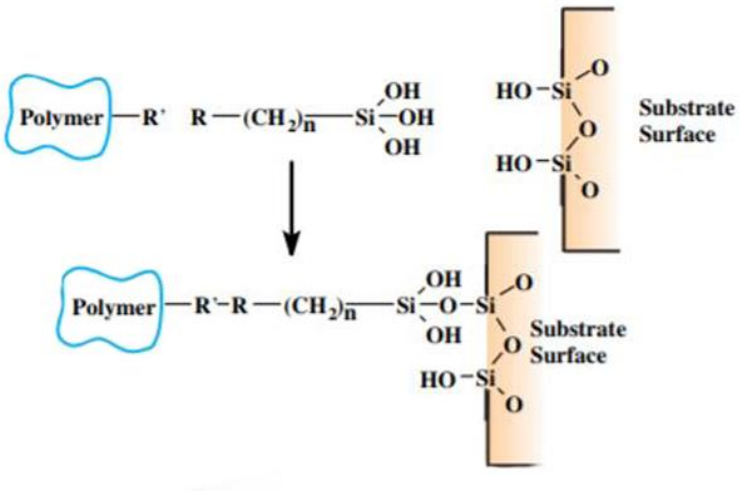

Figure 3 Working of a typical Silane Coupling Agent for bonding an organic Polymer with an inorganic metal substrate[43]

CHAPTER 3

Experimental Setup and Data Collection techniques

Experimental Setup:

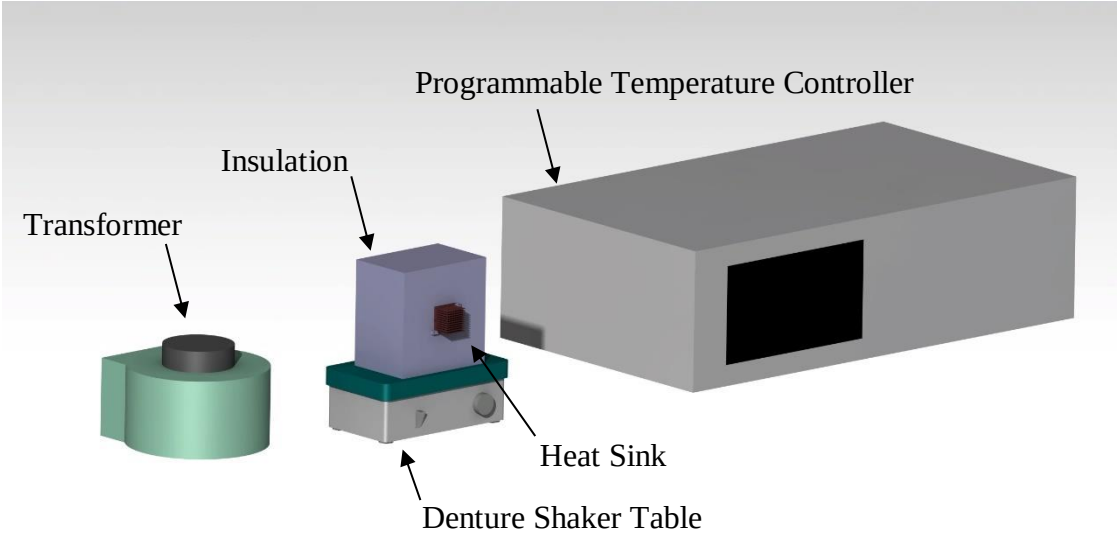

Figure 4 : 3D visualization of the experimental setup arrangement. Note: horizontally arranged Heatsinks.

The experimental setup for testing the heatsinks consisted of a Circuit Specialists variable voltage Variac Transformer of input 110 V AC 60 Hz, a Stanford Research Systems PTC 10 Programmable Temperature Controller for data collection from 4 T type thermocouples and a denture shaker table with fixed frequency of 60 Hz and variable amplitudes.

The experimental setup consisted of a copper block of $38 \times 38 \times 60$ mm with holes drilled for resistance heater to supply a constant heat flux, thermocouples for temperature measurement and mounts to secure heat sink from any motion. The setup is shown in detail in the following figure.

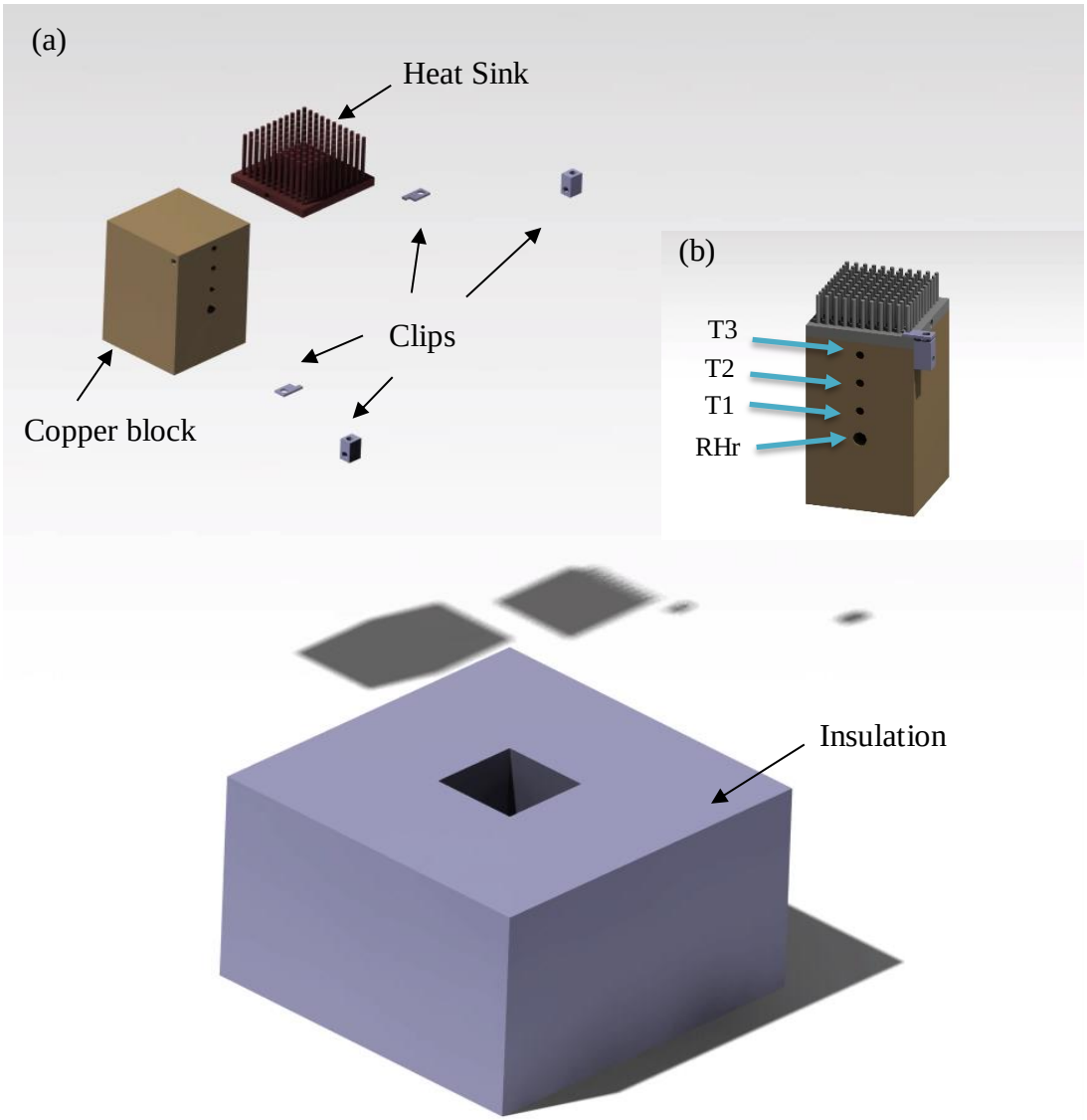

Figure 5: (a) Exploded view of the experimental setup; (b) Locations of different thermocouples indicated by T# and Resistance Heater indicated by RHr

The entire setup was covered with Plexiglass sheets to prevent unnecessary drafts of air from the movements in the surrounding.

T type thermocouples have range around -200 to $400^{o}C$ and accuracy of $\pm\ 1^{o}C$ Hence T type thermocouples were used for temperature measurements. 3 T type

thermocouples were located inside the copper block and 1 T type thermocouple was used to measure ambient temperature.

Data Collection:

Each heatsink was supplied with 10 W power through the resistance heater and allowed to reach its maximum temperature (or within the range of $\pm 1^{o}C$). Once the maximum temperature was reached, the shaker table was turned on and the heatsinks were allowed to vibrate and to reach their steady state temperature. Each test was conduced minimum 3 times for each of the 4 settings of the amplitude of the shaker table. The run time for each test was around 8 hours/test.

For data collection, T type thermocouples were connected to Stanford Research Systems PTC10 programmable temperature controller. This controller had a provision to measure up to 4 thermocouple readings. The Programmable Temperature Controller creates the separate data files in format '.PTC' for each thermocouple. These '.PTC' files were combined into one file and converted to '.csv' and '.xlsx' files using a software called PTCfileConverter. These .xlsx and .csv files were used for further data analysis.

The figure below shows the drop in temperature due to the vibrations generated by the shaker table. The power supplied to the heatsinks through the Variac Transformer was kept constant (10 W) throughout the test and for each of the tests.

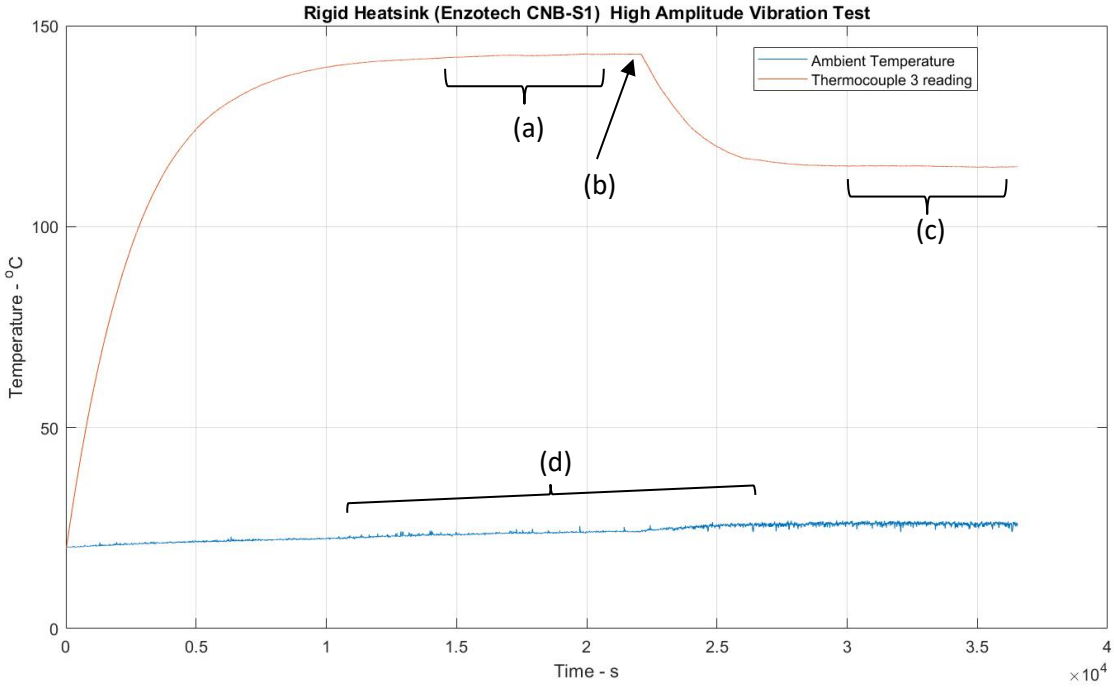

Figure 6 : A typical Thermal-Vibration test reading

In the above plot, part (a) indicates the steady state temperature $143^{o}C$ of the heatsink. Part (b) indicates the point at which the shaker table was turned on and vibrations began at 60 Hz. It was observed that the heatsink experienced drop in the temperature. Part (c) shows the new steady state reached by the heatsink when the shaker table was running. Part (d) indicates the temperature of the surrounding/ambient.

The tests were conducted in the following manner:

Table 2 : Number of Heatsink tests

Heatsink	**Shaker table Setting**	**Tests per setting**	**Total Tests**
Flexible Heatsink 1 (PDMS interface)	Low Amplitude	3	12
	Medium Amplitude		
	High Amplitude		
	Very High Amplitude		
Flexible Heatsink 2 (PDMS + TIM)	Low Amplitude	3	12
	Medium Amplitude		
	High Amplitude		
	Very High Amplitude		
Flexible Heatsink 3 (PDMS + LM)	Low Amplitude	3	12
	Medium Amplitude		
	High Amplitude		
	Very High Amplitude		
Rigid Heatsink Enzotech CNB-S1	Low Amplitude	3	12
	Medium Amplitude		
	High Amplitude		
	Very High Amplitude		
		Total Tests	**48**

During theoretical calculations, the properties of copper were assumed to be close to C11000.[46] CoolProp library was used to evaluate thermophysical properties of the fluids in MATLAB codes.[47]

Vibrations:

The motion that repeats itself after an interval of time is called vibration. During vibrations the potential energy of the system is transferred to a kinetic energy and kinetic energy is transfer to potential energy alternately. The energy is dissipated in each cycle of vibration when the system is damped.[48] An external source of vibration is necessary to maintain the steady state vibrations. The vibrations are classified as follows:

Free vibration: When the system is left to vibrate on its own after an initial vibration then the vibration is known as free vibration. In this case, no external force acts on the system.

Forced vibration: When the system is forced with an external periodical force, the resulting vibrations in the system is termed as forced vibrations.

The amplitude and frequency of vibration in a structure are controlled by the two factors: the excitation applied and response of the structure to that particular excitation. [49] The main sources of excitation are wind, shocks, earthquakes, external sources such as imbalanced machinery etc. And the response of the structure depends on the natural frequency of the structure and inherent level of damping. Though the vibrations are considered undesirable in most of the structures due to the generation of dynamic stresses and strains leading to fatigue failures, these heat sinks are designed purposely to vibrate at maximum amplitudes at their resonance frequencies.

MATLAB Image Detection Technique:

MATLAB was used to characterize vibrations of the shaker table and heat sinks. Image analysis technique was used to track the change in motion of pins in each of images captured by the high-speed camera.

Photron Fastcam Mini UX 100[50] was used to capture the vibrations of the pin fins of the heat sink and the vibrations of the shaker table. With a well-adjusted lighting, a single reading with 500 images were captured at 5000 fps. The distances in the image were calibrated using known distances such as the diameter of the pin fin. The time interval between two images were calculated using the following relation.

$$Time = \frac{number\ of\ corrosponding\ images}{Frames\ per\ second}$$

The time interval between 2 corresponding images was 1/5000 second for a 5000-fps setting.

A function was written in MATLAB to track the centroid of an area of the object (Pin fins, shaker table base) in a manually defined region of interest in the images. This function was semi-automatic i.e. information such as region of interest was entered into this function manually. Region of interest was selected strategically in such a manner that it would track the motion of a single object in the image.

The high-speed camera captures a monochrome black and white image in the RGB format. The RGB image captured by the high-speed camera was converted into a grayscale image. The region of interest was selected manually using rectangular region and stored as a new binary image. The grayscale image was converted into a binary image too. The two binary images were compared using a logical AND operator. This method proved successful in retaining the features/objects in the region of interest and

deleting the objects outside the region of interest. Centroid of an area in the region of interest was tracked for each image to store the X displacement and Y displacement.

MATLABs image batch processing application was used to run this function on every image in a single reading. The X and Y displacements of the centroid of an area were imported in the workspace and plotted against time using a separate code.

The region of interest was fixed for every image in one reading. One drawback of this method was that, due to the moving objects in every image, some images had unwanted objects entering in the region of interest. To tackle this issue, the region of interest was chosen such that the area of unwanted objects in the region of interest would not exceed the area of the object to be tracked. Using a filter, the unwanted areas in the region of interest were removed. This was done to ensure that the MATLAB function tracks only the centroid of the largest area in the region of interest.

A typical data extraction process is explained using the following flow chart:

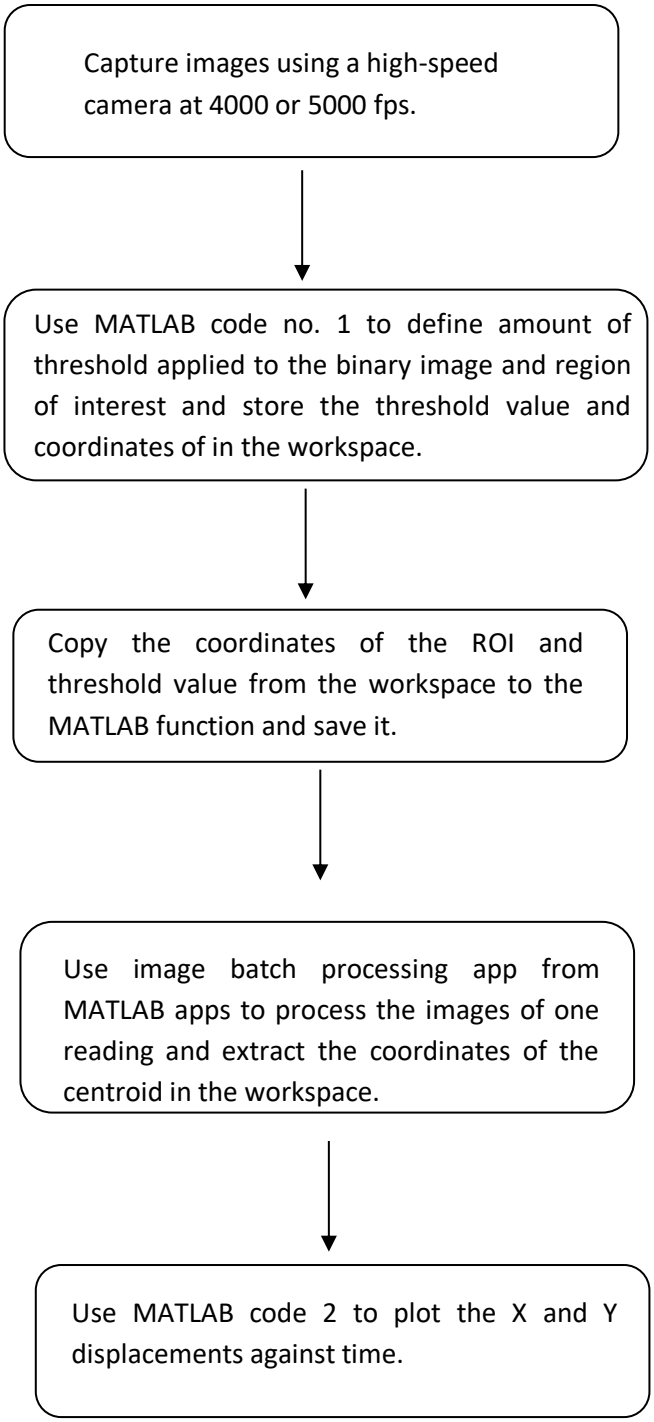

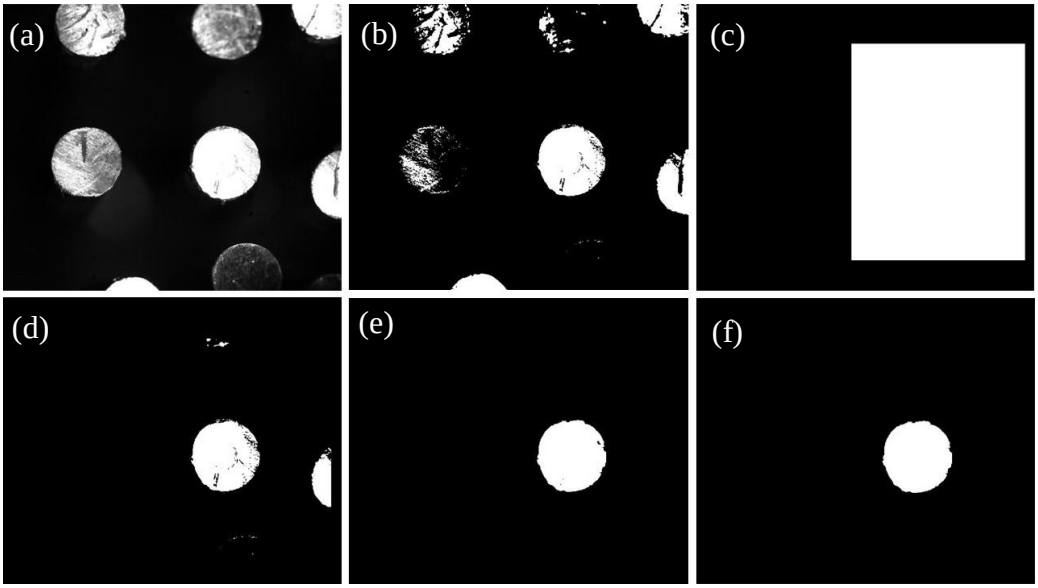

Figure 7 : Working of the MATLAB Code: To get rid of unwanted data from the Image. (a) Original image, (b) Binary Image, (c) definition of Region of interest, (d) Logical AND operation performed on image b and image c, (e) Dilation of edges and selection of largest area, (f) Fill holes.

The above figure demonstrates the steps taken by the MATLAB code to extract desired area from the given image. These 6 steps are implemented on all the images in a particular reading. Using known parameters such as the diameter of the pin fin, distances are calibrated, and the centroid of the desired area is tracked and plotted as shown in the figure 6 to study the characteristics of pin fin vibrations.

The distance between two adjacent images could be used to calibrate time and the distance between two adjacent troughs could be used to measure one complete oscillation.

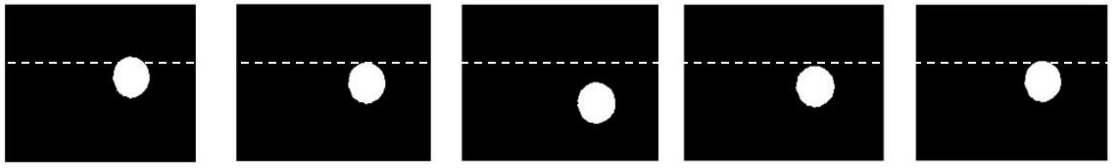

Figure 8: Processed images indicating movement of a flexible pin

Image analysis technique is a faster way to accurately to track x displacements and y displacements of the pin fins. The output of the code could be plotted as follows.

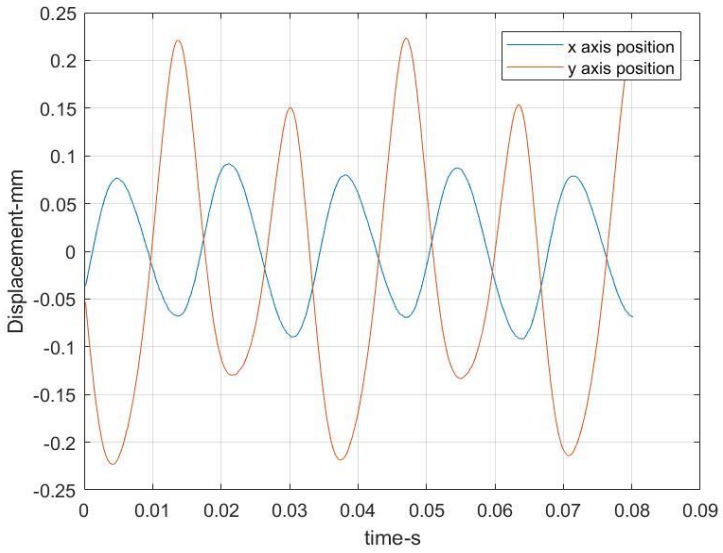

Figure 9 : A typical high-speed camera reading when the shaker table is activated.

This plot indicates that the motion of the pin is not perfectly perpendicular to the y axis. The pin fin vibrates in x and y axis or axis of vibration is $\tan^{-1}\left(\frac{y}{x}\right) = 76.26^{o}$ to the x axis for the first period and 65.1^{0} for the second period. This indicates that the pins are tracing an elliptical path. It can also be observed that the vibration of the pins is not perfectly uniform.

CHAPTER 4

Analytical Study

Natural Frequency of a flexible pin fin.

To calculate the free natural vibrations of the flexible pins, the pin was left from a specific amplitude and allowed to vibrate own until it became stationary. The image analysis technique explained above was used to track the centroid of the area.

Here edge detection method was implemented. Threshold filtering, Sobel approximation, Prewitt approximation and Canny approximation were implemented for edge detection as necessary according to the lighting setup and gradient for each test. [51]–[61]

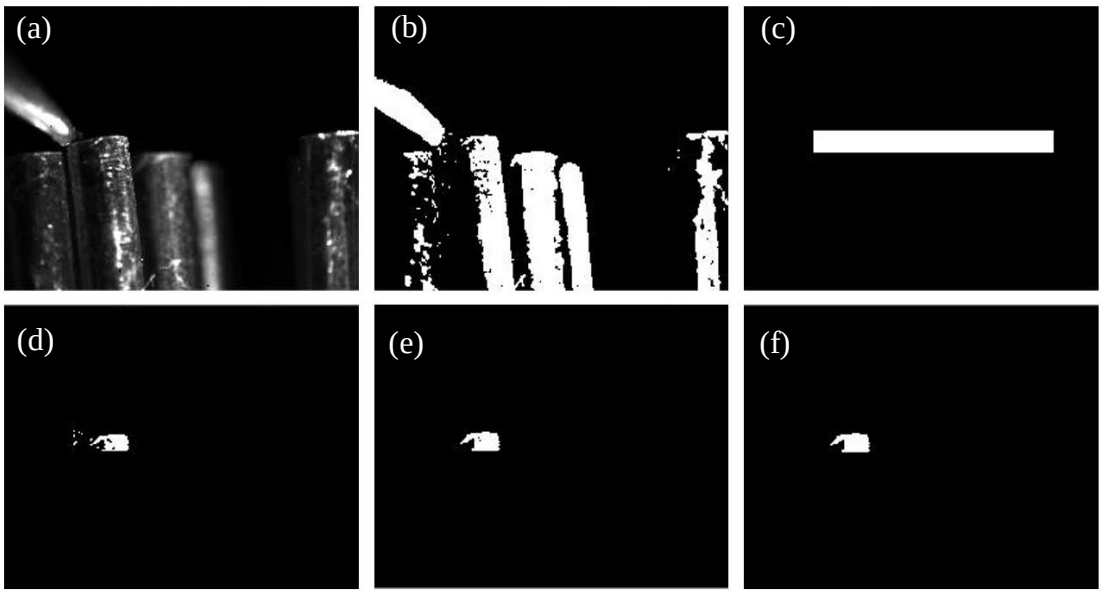

Figure 10: Working of the MATLAB Code: (a) Original image, (b) Original image converted to a binary image, (c) Region of interest defined, (d) Logical AND operation performed on image 2 and image 3 to get rid of unwanted data from the image, (e) Dilation of edges and selection of largest area (f) Fill holes if any.

The output of the above code was used to track the tip of the pin fin and it was observed that the pin fin perfectly traced a damped oscillation. The output of the code was plotted as follows:

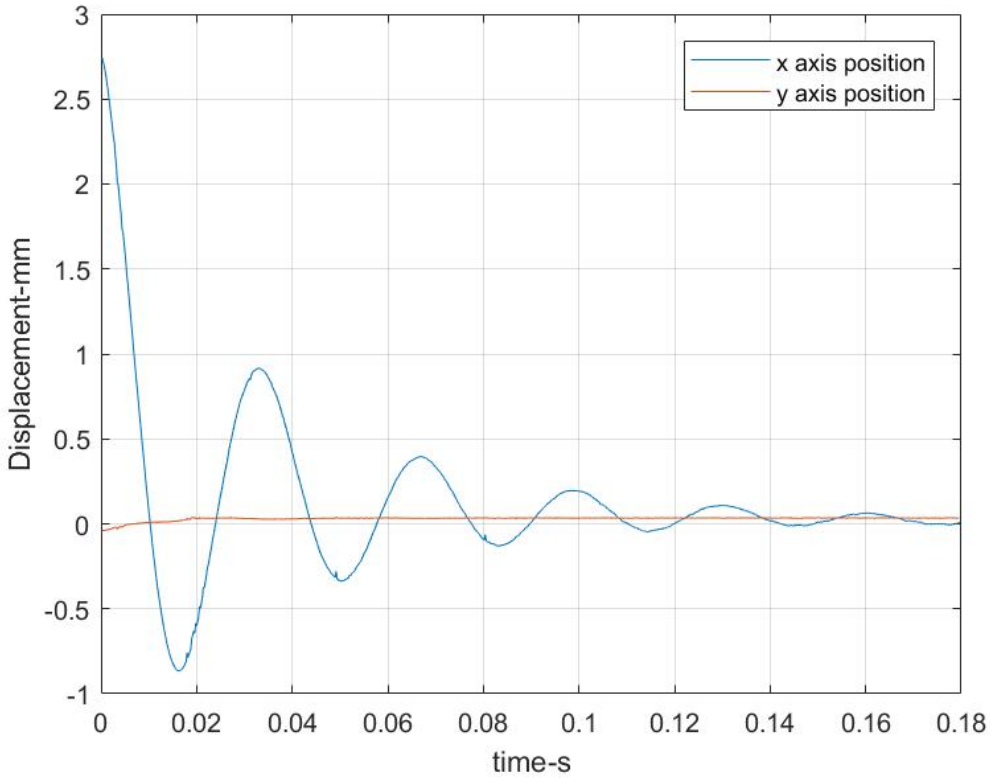

Figure 11 : A typical reading obtained from a high-speed camera

Reference books on vibrations were used to characterize these vibrations.[48], [49], [62]–[64] The logarithmic decrement denoted by δ is represented by the following equation:

$$\delta = In\left(\frac{x(t)}{x(t+T_d)}\right) \quad (1)$$

Where $x(t)$ is position of the tip of the pin at time t and $T_d$is the period of oscillation. The displacement of oscillation is given by the following equation:

$$x(t) = Ae^{-\zeta\omega_n t}\sin(\omega_d t + \phi) \quad (2)$$

Where A is the amplitude of vibration, ζ is the dimensionless damping ratio, t is the time-period, ϕ is the possible phase shift, $\omega_n$is the undamped natural frequency and $\omega_d$is the damped natural frequency.

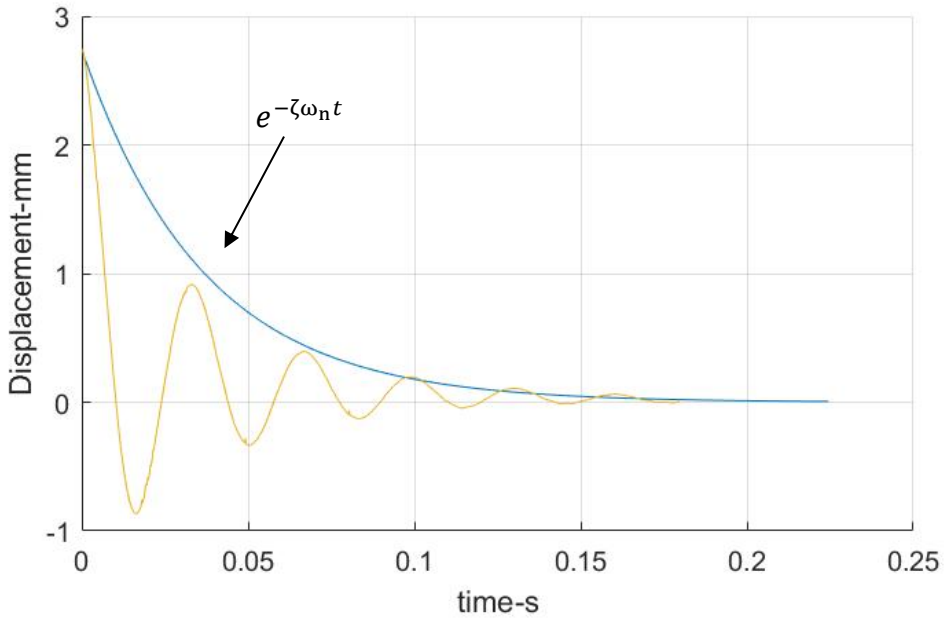

Figure 12: blue line indicating logarithmic decrement

Substituting $x(t)$ in the logarithmic decrement

$$\delta = In\left(\frac{x(t)}{x(t+T_d)}\right) = In\left(\frac{Ae^{-\zeta\omega_n t}\sin(\omega_d t + \phi)}{Ae^{-\zeta\omega_n (t+T_d)}\sin(\omega_d t + \omega_d T_d + \phi)}\right) = Ine^{\zeta\omega_n T_d} \quad (3)$$

$$= \zeta\omega_n T_d$$

Further evaluating

$$\delta = \zeta\omega_n T_d = \frac{2\pi\zeta}{\sqrt{1-\zeta^2}} \quad (4)$$

Which gives

$$\zeta = \frac{\delta}{\sqrt{4\pi^2 + \delta^2}} \tag{5}$$

The damped natural frequency is given by the following equation:

$$\omega_d = \omega_n \sqrt{1 - 2\zeta^2} \tag{6}$$

Analytical model of a pin fin:

The flexible pin fin can be modelled as a uniform circular cross section beam with one end spring hinged and the other end connected to a translational spring. Work on these problems were previously carried out by various researchers. In this report, Chun's model and Zhong et. al. model will be used.

Maurizi et. al. proposed a study to deal with the free vibration of a beam hinged at one end by a rotational spring and a translational spring at the other end. [65]

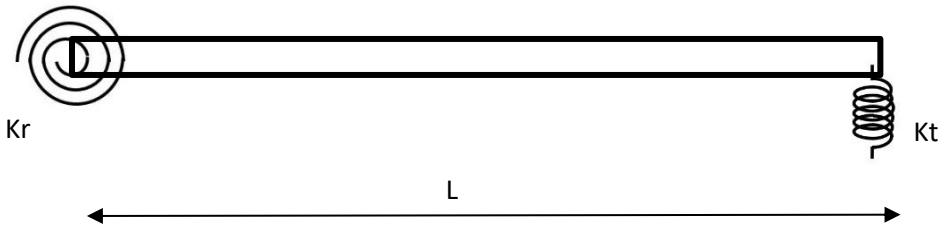

Figure 13: Cantilever beam with one end connected to a rotational spring and other end connected to a translational spring

The differential equation for the free vibrations of a uniform cantilever beam is given as (7)

$$EI \frac{\delta^4 y}{\delta x^4} + m \frac{\delta^2 y}{\delta t^2} = 0$$

Here, EI is the modulus of flexural rigidity of the beam, y is the deflection of the beam, m is mass per unit length, x is the distance from the spring-hinged side and t represents time.

This is subjected to the following boundary conditions,

At x=0,

$$y(0,t) = 0, \qquad K_r \frac{\delta y(0,t)}{\delta x} = EI \frac{\delta^2 y(0,t)}{\delta x^2} \tag{8}$$

At x= L,

$$\frac{\delta^2 y(L,t)}{\delta x^2} = 0, \qquad EI \frac{\delta^3 y(L,t)}{\delta x^3} = K_t y(L,t) \tag{9}$$

K_r and K_t are the rotational and translational spring constants respectively.

Following separation of variables, one could assume the following form of solution,

$$y(x,t) = \sum_{n=1}^{\infty} G_n(x) T(t) \tag{10}$$

$G_n(x)$ is the n th mode of natural vibration and

$$G_n(x) = A_n \cos(C_n x) + B_n sin(c_n x) + C_n cosh(c_n x) + D_n sinh(c_n x)\,, \tag{11}$$

$$C_n^4 = \left(\frac{y_n}{L}\right)^4 = \omega_n^2 \left(\frac{m}{EI}\right) \tag{12}$$

Substituting $G_n(x)$ in $y(x,t)$ and later in the boundary conditions one could obtain a system of linear homogenous equations which could be converted into the following frequency equation:

$$\begin{aligned}
&\left(\frac{E^2 I^2}{K_r K_t L^4}\right)(C_n L)^4 \left[sin(C_n L)\cosh(C_n L) - \sinh(C_n L)\cos(C_n L)\right] \\
&\quad - \left(\frac{EI}{K_t L^3}\right)(C_n L)^3 [cos(C_n L)\cosh(C_n L) + 1] \\
&\quad - \left(\frac{2EI}{K_r L}\right)(C_n L)[sin(C_n L)\sinh(C_n L)] \\
&\quad - [sin(C_n L)\cosh(C_n L) - \sinh(C_n L)\cos(C_n L)] = 0
\end{aligned} \tag{13}$$

The natural frequency for the n^{th} mode is given as,

$$f_n = \frac{C_n^2 L^2}{2\pi}\sqrt{\frac{EI}{mL^4}} \tag{14}$$

K. R. Chun modelled a beam with one end hinged with a rotational spring and the other end free. [66]

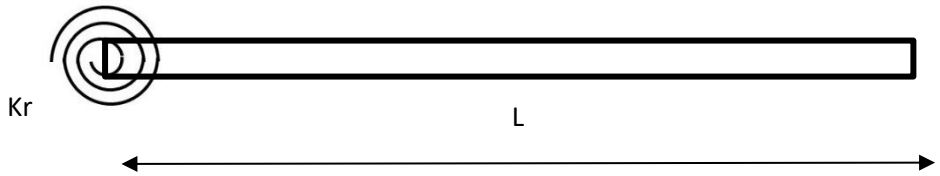

Figure 14: Cantilever beam connected to a rotational spring

For a simple torsion (rotational) spring-end and free end system the above equation (15) reduces to,

$$\left(\frac{K_r L}{EI}\right)\left(\frac{1}{(C_n L)}\right)[cos(C_n L)\cosh(C_n L)+1]-[sin(C_n L)\cosh(C_n L) - \sinh(C_n L)\cos(C_n L)] = 0 \tag{16}$$

Where , $I = \frac{\pi d^4}{64} = 3.727 \times 10^{-13}\ m^4$, $E = 117 \times 10^9\ Pa$, $L = 25.4 \times 10^{-3} m$, $m = \rho A = 0.0194\ Kg/m$

$$f_n = \frac{(C_n L)^2}{2\pi}\sqrt{\frac{EI}{mL^4}} \tag{17}$$

Zhong et. al. used a similar concept in their model to evaluate equivalent stiffness of flexible supports on the MEMS cantilever-based supports. [67]

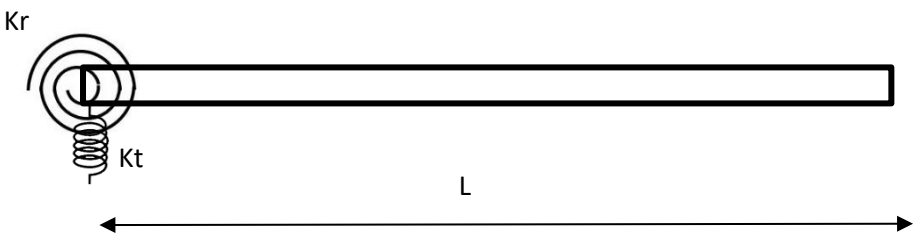

Figure 15 : Cantilever beam with the end connected to a rotational spring and a translational spring.

could be expressed as,

$$EI\frac{\delta^4 y}{\delta x^4} + m\frac{\delta^2 y}{\delta t^2} + \frac{EA}{2L}\frac{\delta^2 y}{\delta x^2}\int_0^L \left(\frac{\delta y}{\delta x}\right)^2 dx + c\frac{\delta y}{\delta t} = Fcos(\Omega t) \tag{18}$$

Where $y = y(x,t)$, $\Omega = 2\pi n$; n= frequency of vibration (Hz)

Subjected to the following boundary conditions:

At x = 0

$$EI\frac{\delta^2 y}{\delta x^2} - K_r\frac{\delta y}{\delta x} = 0, \text{ and } -\frac{\delta}{\delta x}\left(\frac{\delta^2 y}{\delta x^2}\right) - K_r y = 0 \tag{19}$$

At x = L

$$\frac{\delta^2 y}{\delta x^2} = 0, \text{ and } \frac{\delta}{\delta x}\left(\frac{\delta^2 y}{\delta x^2}\right) = 0 \tag{20}$$

The algebraic system of equations for the resonance frequencies are as follows:

$$\begin{vmatrix} \sqrt{\omega} & \alpha_R & -\sqrt{\omega} & \alpha_R \\ \alpha_T & -\omega^{\frac{3}{2}} & \alpha_R & \omega^{\frac{3}{2}} \\ cos\sqrt{\omega} & sin\sqrt{\omega} & -cosh\sqrt{\omega} & -sinh\sqrt{\omega} \\ sin\sqrt{\omega} & -cos\sqrt{\omega} & sinh\sqrt{\omega} & cosh\sqrt{\omega} \end{vmatrix} = 0 \tag{21}$$

Where, $\alpha_R = \frac{K_r L}{EI}$ and $\alpha_t = \frac{K_t L^3}{EI}$ and $\omega = 2\pi f_n$, fn = resonance frequency (Hz)

From image analysis the values of natural frequency of the pin fin for mode 1 was calculated. Using these natural frequency values, one could calculate stiffness of the bonding structure which depends on the geometry and material properties.

For example,

For Maurizi's model,

$$\left(\frac{K_r L}{EI}\right)\left(\frac{1}{(C_n L)}\right)[cos(C_n L)\cosh(C_n L)+1]-[sin(C_n L)\cosh(C_n L) - \sinh(C_n L)\cos(C_n L)]=0 \tag{22}$$

This equation as multiple solutions. One way to extract required solution from this equation is substituting this equation as a function and plotting it for various values of $C_n L$.

$$f(C_n L)=\left(\frac{K_r L}{EI}\right)\left(\frac{1}{(C_n L)}\right)[cos(C_n L)\cosh(C_n L)+1] - [sin(C_n L)\cosh(C_n L) - \sinh(C_n L)\cos(C_n L)] \tag{23}$$

Plotting $f(C_n L)$

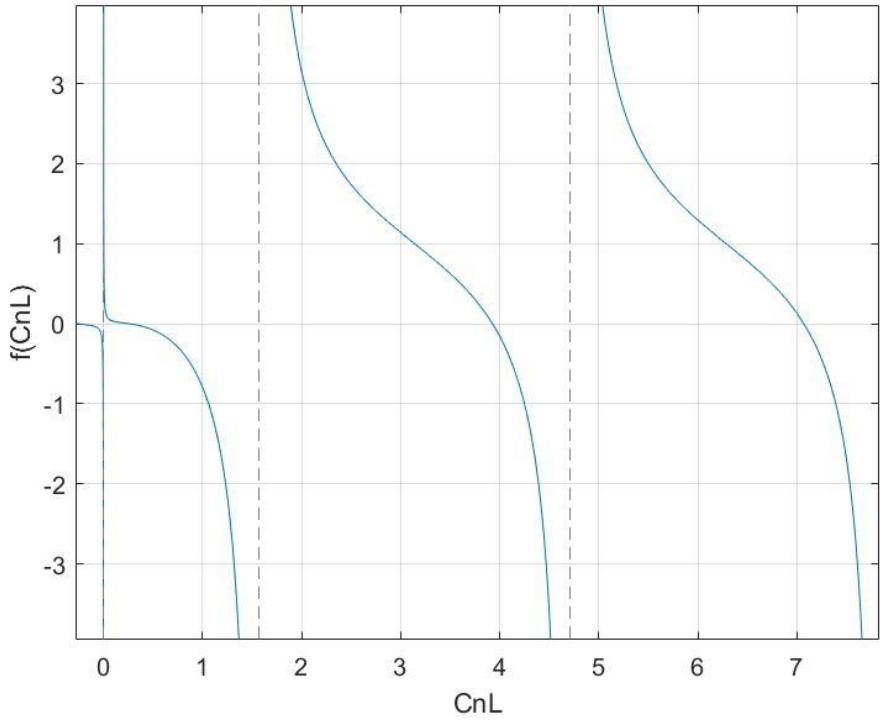

Figure 16: Solution of f(CnL) at various CnL values

For first mode $C_nL = 0.2599$, at stiffness 2.615 N/mm.

$$f_n = \frac{(C_nL)^2}{2\pi}\sqrt{\frac{EI}{mL^4}} = 24.98Hz$$

Similarly, for Zhong's model,

$$\begin{vmatrix} \sqrt{\omega} & \alpha_R & -\sqrt{\omega} & \alpha_R \\ \alpha_T & -\omega^{\frac{3}{2}} & \alpha_R & \omega^{\frac{3}{2}} \\ cos\sqrt{\omega} & sin\sqrt{\omega} & -cosh\sqrt{\omega} & -sinh\sqrt{\omega} \\ sin\sqrt{\omega} & -cos\sqrt{\omega} & sinh\sqrt{\omega} & cosh\sqrt{\omega} \end{vmatrix} = 0 \quad (24)$$

Substituting this equation as a function of ω

$$\begin{vmatrix} \sqrt{\omega} & \alpha_R & -\sqrt{\omega} & \alpha_R \\ \alpha_T & -\omega^{\frac{3}{2}} & \alpha_R & \omega^{\frac{3}{2}} \\ cos\sqrt{\omega} & sin\sqrt{\omega} & -cosh\sqrt{\omega} & -sinh\sqrt{\omega} \\ sin\sqrt{\omega} & -cos\sqrt{\omega} & sinh\sqrt{\omega} & cosh\sqrt{\omega} \end{vmatrix} = f(\omega) \quad (25)$$

Plotting $f(\omega)$

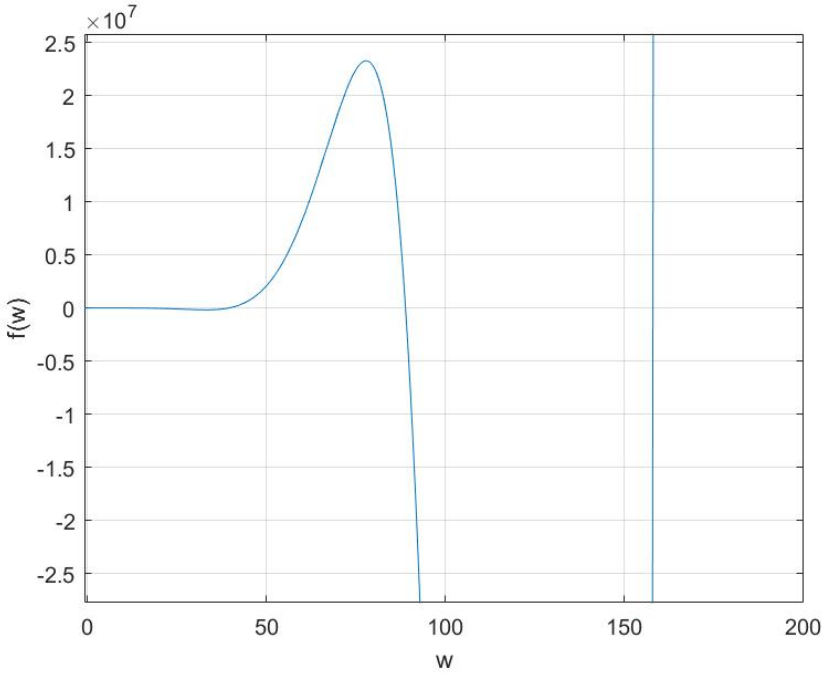

Figure 17: Solution of f(ω) at various values of ω

For the stiffness 2.615 N/mm it was observed that the flexible pin vibrates at

$$\omega_4 = 157.913 \frac{rad}{s}$$

$$f_n = \frac{\omega}{2\pi} = 25.13\ Hz$$

Setting the stiffness value 2.615 N/mm following results,

Table 3 : Difference between Maurizi's Model and Zhong's Model

Model	**Stiffness K = Kr = Kt**	**Natural frequency**
Maurizi's model	0.00262 N/m	25.0 Hz
Zhong's model	0.00262 N/m	25.1 Hz
Experimental Value	-	25.1 Hz

Heat Transfer model

Natural Convection:

Horizontally Pin fin heatsinks can be modelled as a vertical plate and horizontal cylinders. Calculations were done using MATLAB. CoolProp was used to obtain fluid properties at varying temperatures.

The total heat dissipation of the heat sink is usually done as follows

$$Q_{total} = Q_{plate} + Q_{pins} = \left(h_{plate}A_{plate} + \eta_{pins}h_{pins}A_{pins}\right)(T_s - T_{air}) \qquad (26)$$

Efficiency of the pin is given by

$$\eta_{pin} = \frac{\tanh(mL)}{mL} \tag{27}$$

Where

$$m = \sqrt{\frac{4h_{pins}}{K_{cu}d}} \tag{28}$$

Nusselt number is defined using following equation:

$$Nu = \frac{hL}{K_{air}} \tag{29}$$

Nusselt number for a vertical plate is obtained by the following equation[68][69],

$$Nu_{plate} = 0.825 + \frac{0.387Ra^{\frac{1}{6}}}{\left(1 + \left(\frac{0.492}{Pr}\right)^{\frac{9}{16}}\right)^{\frac{8}{27}}} \tag{30}$$

Where,

$$Ra_{plate} = \frac{g\beta(T_s - T_{air})L_c^3}{\nu\alpha} \tag{31}$$

Nusselt number for a horizontal pin fin is given as[68][69]:

$$Nu_{pin} = 0.6 + \frac{0.387Ra^{\frac{1}{6}}}{\left(1 + \left(\frac{0.559}{Pr}\right)^{\frac{9}{16}}\right)^{\frac{8}{27}}} \tag{32}$$

Where,

$$Ra_{pin} = \frac{g\beta(T_s - T_{air})L_c^3}{\nu\alpha} \tag{33}$$

Plugging 32 and 30 in 29, one could get the value to h for the pin fin and the base plate.

The above method of calculating h for single pinfin and multiplying by total number of pin fins to obtain overall heat transfer is termed as traditional method in this report.

Joo et. al. argued and claimed[70] that

$$h_{pin} = \frac{S_h S_v}{\pi d L} \frac{(4 S_h S_v - \pi d^2)}{48} \frac{\rho_f C_p g \beta \eta_{fin} (T_b - T_{air})}{\nu_f} \quad (34)$$

Table 4: Comparison between the traditional method and Joo's observation

Method of calculation	**Calculated Q_{total}**	**Experimental Q_{total}**
Traditional method	42.8 W	10.2 W
Joo's Model	10.3 W	10.2 W

The traditional method does not consider the effects the densely packed pin fins hence overestimates the heat transfer. Joo's Model considers the array of pin fins as densely packed porous medium. [70] Thus it obtains fairly accurate results.

Vibration induced Forced Convection:

Robert Lemlich conducted a series of tests on electrically heated wires[16] and he approximated Nusselt number relation of horizontally heated wires as follows:

$$Nu = \left[0.75 + \frac{0.0022(Re^{2.05}(\beta \Delta T)^{0.33})}{Pr^{1.54} Gr^{0.41}}\right][0.63 + 0.35(Gr \times Pr)] \quad (35)$$

Here $Re = \frac{VD}{\nu}$

The velocity of the pin fins was calculated using the relation $V = 2Af_n$

Where 2A is the peak-to-peak amplitude of vibration and f_n is the frequency of vibration.

Using above analytical models one could predict the change in temperature at varying heat transfer.

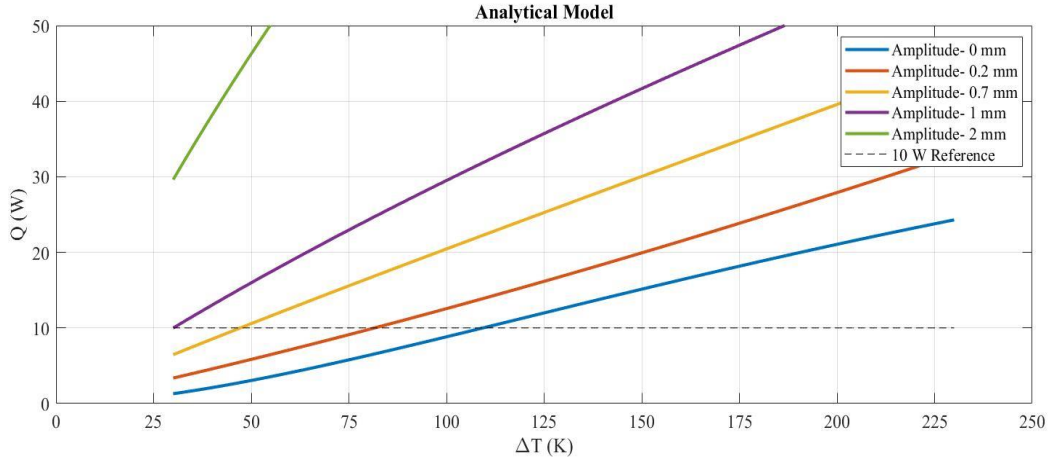

Figure 18 Prediction of Temperature difference with respect to heat transfer

From the above figure, it could be observed that the predicted thermal resistance $R = \frac{\Delta T}{Q}$ is in the range of 10.8 K/W to 3.1 K/W for range of input shaker table amplitude of 0 to 1 mm.

CHAPTER 5

Results and Discussion

Effect of vibration on thermal Resistance:

Experimental data is shown in the plots below.

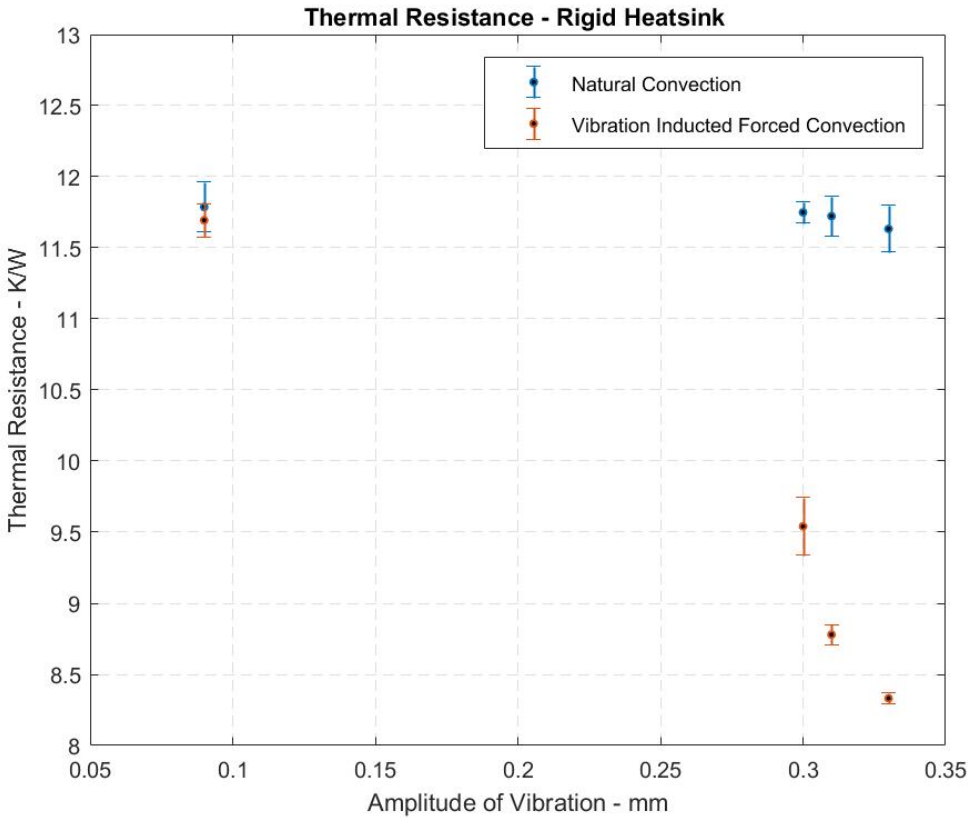

Figure 19 : Thermal Resistance of Rigid Heatsink Enzotech CNB-S1. [The error bars were calculated using 1 standard deviation]

In the above plot, blue ticks indicate thermal resistance during the steady nonvibrational case of natural convection. Red ticks show the steady thermal resistances during the active steady vibrations using the shaker table.

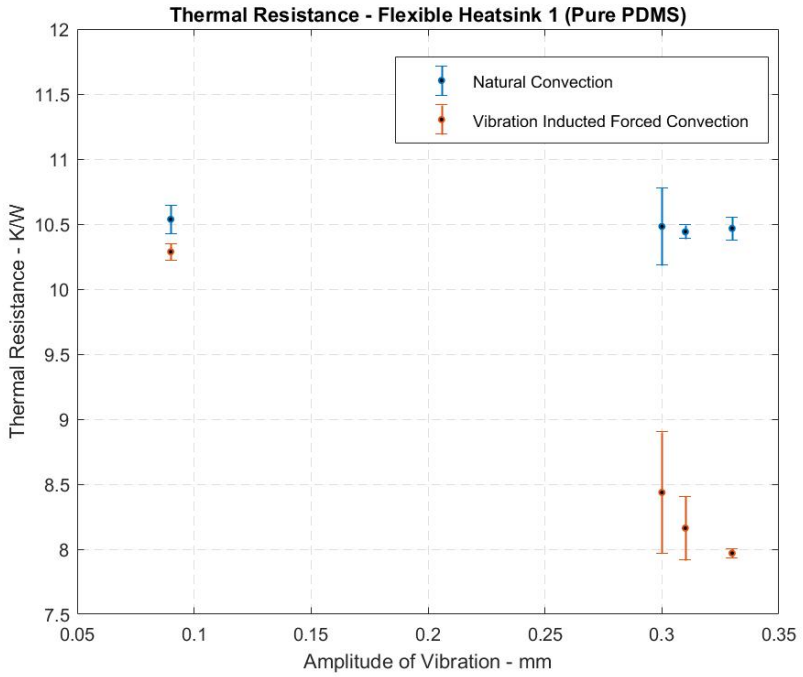

Figure 20 : : Thermal Resistance of Flexible heatsink 1 (PDMS). [The error bars were calculated using 1 standard deviation]

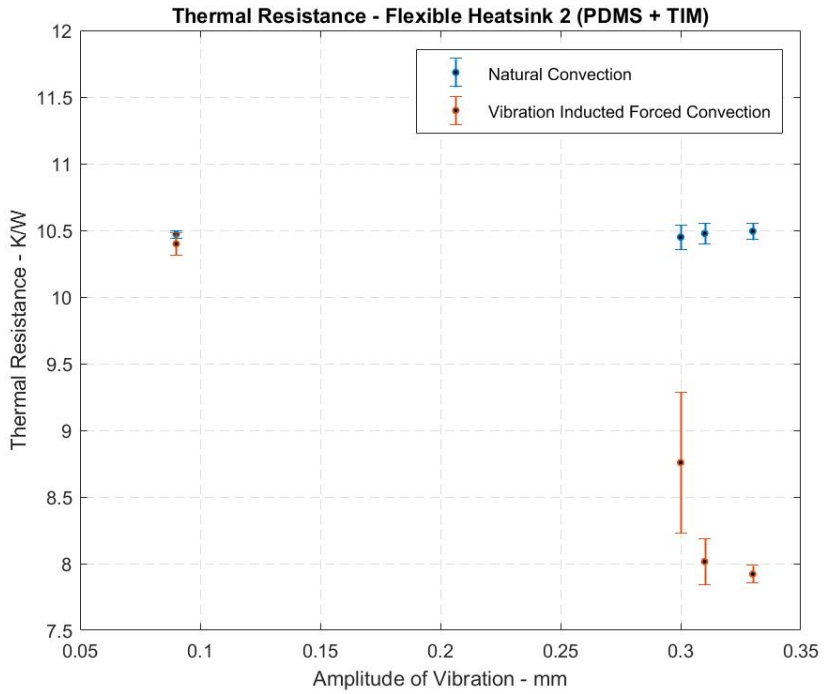

Figure 21 : Thermal Resistance of Flexible heatsink 2 (PDMS + TIM). [The error bars were calculated using 1 standard deviation]

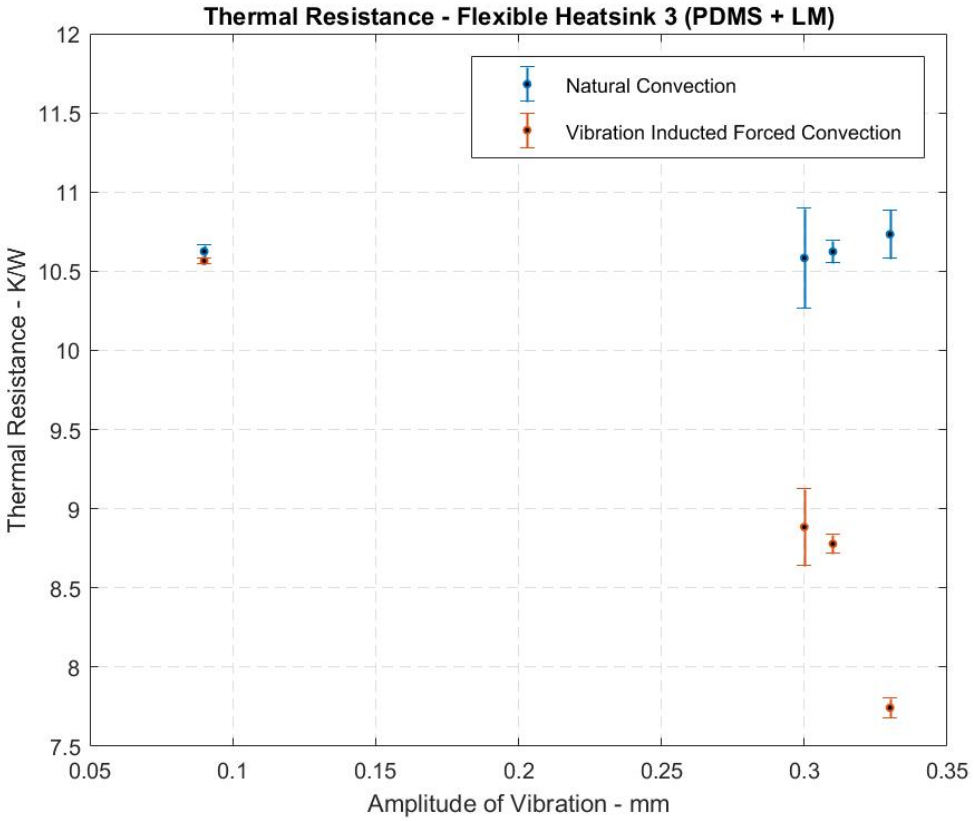

Figure 22 : Thermal Resistance of Flexible heatsink 3 (PDMS + LM). [The error bars were calculated using 1 standard deviation]

The blue markers indicate the thermal resistance of the heatsink during the natural convection i.e. the static no-vibration case and the red markers indicate thermal resistance during vibration induced forced convection. According to the experimental results, 23% decrease in the thermal resistance of the Flexible heatsink 1 was observed at the largest value of amplitude while 24% decrease in the thermal resistance as observed in Flexible heatsink 2 at the largest value of amplitude. 27% decrease in the thermal resistance was observed in the Flexible heatsink 3. While 28% decrease in thermal resistance was observed in the case of Rigid Enzotech CNB S1 at the largest vibration amplitude.

It can be observed that the drop in thermal resistance of all the Flexible heatsinks is less than the rigid heatsink thermal resistance drop. This can be due to the lower amplitudes of vibration of the flexible pin fins. Using image analysis technique it was observed that the flexible pin fins were vibrating at much lesser amplitudes than the input amplitudes of the shaker table.

The thermal resistance was calculated using the Temperatures obtained from the thermal tests.

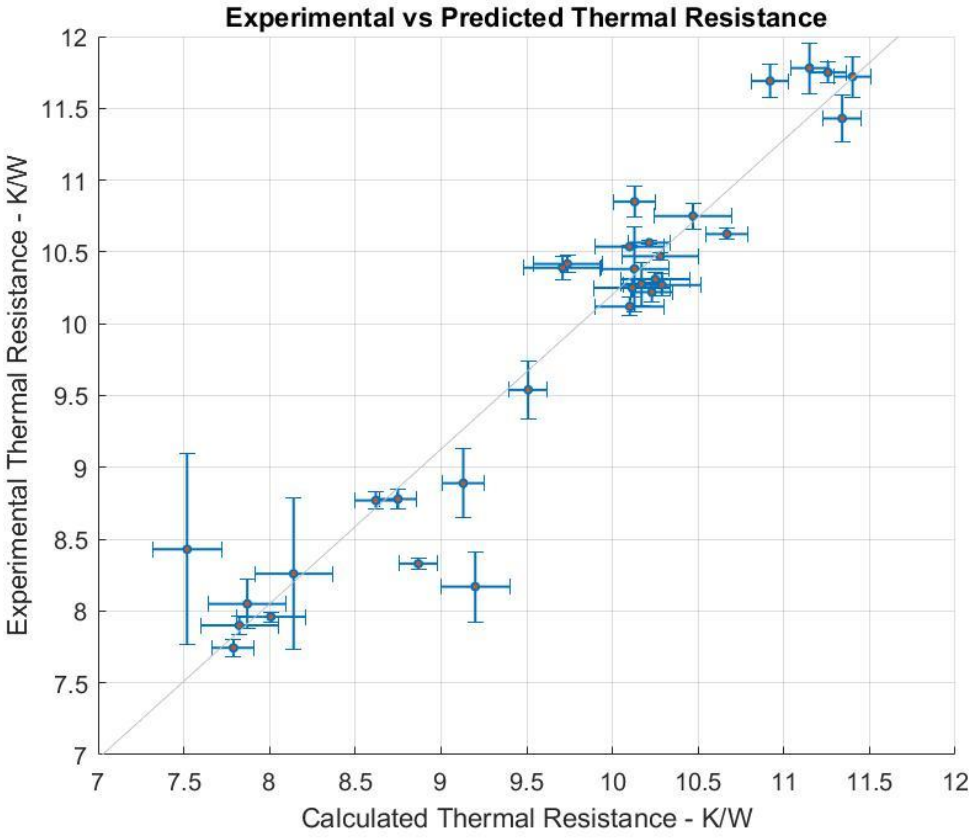

Figure 23 : Experimental results vs Predicted Results, Note: Error bars were calculated using 1 standard deviation.

The experimental and analytical models are in good agreement with each other. It can be observed that there is large variation in calculated data due to the fluctuations

in thermocouple readings during the vibration test as compared to the natural convection tests.

Natural Frequency of pin fins:

Using the method discussed in chapter 4, following results were obtained:

Table 5 : Natural Frequency of the pin fins calculated using high speed camera and MATLAB image analysis technique

Heatsink	***Natural Frequency***	***Damped Natural Frequency***
Flexible Heatsink 1	$\omega_n = 159.97\, rad/s$	$\omega_d = 154.13\, rad/s$
	$F_n = 25.46\, Hz$	$F_d = 24.53\, Hz$
Flexible Heatsink 2	$\omega_n = 138.85\, rad/s$	$\omega_d = 128.30\, rad/s$
	$F_n = 22.09\, Hz$	$F_d = 20.41\, Hz$
Flexible Heatsink 3	$\omega_n = 146.8\, rad/s$	$\omega_d = 142.00\, rad/s$
	$F_n = 23.37\, Hz$	$F_d = 22.60\, Hz$

Note: The values indicated in the above table may have around $\pm$10% error.

It could be said that all the Flexible Heatsinks had natural frequencies in the range of 20 Hz to 30 Hz. The shaker table vibration frequency was limited to 60 Hz which, in some cases, made the flexible pins vibrate at much lower amplitudes than the input amplitudes from the shaker table.

The relation between the stiffness of material forming the bond between pin fins and the copper base plate and their natural frequency is shown in the plot below.

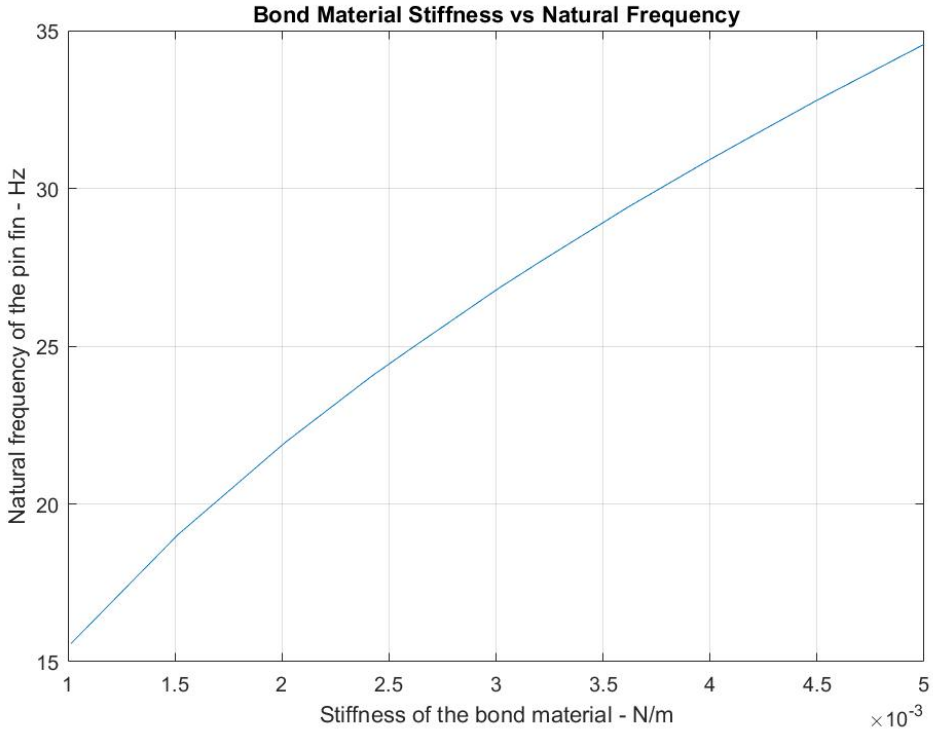

Figure 24 : Effect of bond material stiffness on the natural frequency of the pin fin

Maurizi's model was implemented in figure 22 to track the relation between the rotational stiffness of the material and the natural frequency of the pin fin.

CHAPTER 6

Conclusion and Future Scope

Conclusion:

It can be concluded that the vibration plays a significant role in decreasing the thermal resistance of the heatsinks. It was observed that amplitudes of vibration played a key role in determining the thermal resistance of the different heat sinks. As the amplitude of vibrations increased at a constant frequency, 2 - 3 K/W reduction in overall thermal resistance was observed. At 60Hz of frequency of vibration, rigid heat sink had a lower resistance than the flexible heat sinks because the flexible heat sinks were observed to be vibrating at lower amplitudes than the rigid heat sink. This can be due to the fact that flexible heatsinks were not vibrating at resonance frequency. The natural frequencies of all the flexible heatsinks were in the range of 20 – 30 Hz while the input shaker table frequency was fixed to 60 Hz. This indicates that the flexible heatsinks were vibrating with phase difference above 90^{o} with respect to the shaker table. Due to the limitation of the shaker table, the effects of variable frequencies of vibrations could not be explored in detail.

Future Scope:

A light weight setup with lighter heating element can to be fabricated and used with piezo transducers. Heat sink with very few pin fins and light weight plate (surface) heater can be used to perform future tests. Tactile transducers capable of working at lower variable frequencies can be used to fabricate a custom shaker table. Tactile transducers usually work with standard audio jack. This could facilitate the use of Wolfram Mathematica to generate the audio sin signals of any frequency using its audio signal processing.

By observing the trend of the rigid heatsink thermal resistance, it can be clearly observed that thermal resistance of a device is a function which is inversely proportional to the amplitude of vibrations.

These tests are expected to generate results at various frequencies of vibration thus throwing some light on the effects of flexible heat sink vibrations at resonance frequency. These tests are expected to generate lowest thermal resistances at resonance frequencies.

REFERENCES

[1] M. Ghalambaz, E. Jamesahar, M. A. Ismael, and A. J. Chamkha, "Fluid-structure interaction study of natural convection heat transfer over a flexible oscillating fin in a square cavity," *Int. J. Therm. Sci.*, vol. 111, pp. 256–273, 2017.

[2] K. Khanafer, "Comparison of flow and heat transfer characteristics in a lid-driven cavity between flexible and modified geometry of a heated bottom wall," *Int. J. Heat Mass Transf.*, vol. 78, no. 0, pp. 1032–1041, 2014.

[3] J. S. Go *et al.*, "Heat transfer enhancement using flow-induced vibration of a microfin array," *Sensors Actuators, A Phys.*, pp. 232–239, 2001.

[4] M. K. Iyer *et al.*, "Thermal Design of Heat Spreader and Analysis of Thermal Interface Materials," in *2002 Electronic Components and Technology Conference*, 2002, pp. 1119–1123.

[5] K. Shoele and R. Mittal, "Computational study of flow-induced vibration of a reed in a channel and effect on convective heat transfer," *Phys. Fluids*, vol. 26, no. 12, pp. 1–24, 2014.

[6] K. Horiuchi, A. Nishihara, and K. Sugimura, "Multi-objective optimization of water-cooled pinfin heatsinks," *Int. J. Heat Mass Transf.*, vol. 81, pp. 760–766, 2015.

[7] J. Wakil, "Thermal performance impacts of heat spreading lids on flip chip packages: With and without heat sinks," *Microelectron. Reliab.*, vol. 46, no. 2–4, pp. 380–385, 2006.

[8] A. Rips, K. Shoele, A. Glezer, and R. Mittal, "Efficient electronic cooling via flow-induced vibrations," *Annu. IEEE Semicond. Therm. Meas. Manag. Symp.*, pp. 36–39, 2017.

[9] B. Dagan and E. D. Online, "For More Efficient Cooling, Try Splayed Pin-Fin Heatsinks."

[10] L. Covert, "Dual Function Heatsink Antennas for High Density Three Dimensional Integration of High-Power Transmitters," University Of Florida, 2003.

[11] H. E. Ahmed, B. H. Salman, A. S. Kherbeet, and M. I. Ahmed, "Optimization of thermal design of heat sinks: A review," *Int. J. Heat Mass Transf.*, vol. 118, pp. 129–153, 2018.

[12] R. W. Knight, J. S. Goodling, and D. J. Hall, "Optimal Thermal Design of Forced Convection Heat Sinks-Analytical," *J. Electron. Packag.*, vol. 113, no. 3, p. 313, 2008.

[13] K. Azar and C. D. Mandrone, "Effect of Pin Fin Density of the Thermal Performance of Unshrouded Pin Fin Heat Sinks," *J. Electron. Packag.*, vol. 116,

no. 4, p. 306, 2008.

[14] G. Maranzana, I. Perry, D. Maillet, and S. Raël, "Design optimization of a spreader heat sink for power electronics," *Int. J. Therm. Sci.*, vol. 43, no. 1, pp. 21–29, 2004.

[15] T. Crittenden, S. Jha, and A. Glezer, "Forced Convection Heat Transfer Enhancement in Heat Sink Channels Using Aeroelastically Fluttering Reeds," *IEEE ITHERM Conf.*, vol. 16th, no. 978-1-5090-2994–5, 2017.

[16] R. Lemlich, "Correction: Effect of Vibration on Natural Convective Heat Transfer," *Ind. Eng. Chem.*, vol. 53, no. 4, p. 314, 1961.

[17] J. B. Lee, S. G. Park, B. Kim, J. Ryu, and H. J. Sung, "Heat transfer enhancement by flexible flags clamped vertically in a Poiseuille channel flow," *Int. J. Heat Mass Transf.*, vol. 107, pp. 391–402, 2017.

[18] R. H. Keil, M. H. I. Baird, and R. H. Keil, "Enhancement of Heat Transfer by Flow Pulsation," *Ind. Eng. Chem. Process Des. Dev.*, vol. 10, no. 4, pp. 473–478, 1971.

[19] Z. Li *et al.*, "Bio-inspired self-agitator for convective heat transfer enhancement," *Appl. Phys. Lett.*, vol. 113, no. 11, 2018.

[20] R. K. B. Gallegos and R. N. Sharma, "Flags as vortex generators for heat transfer enhancement: Gaps and challenges," *Renew. Sustain. Energy Rev.*, vol. 76, no. October 2016, pp. 950–962, 2017.

[21] P. Kumar *et al.*, "Heat Transfer Intensification and Flow rate Control in Dynamic Micro-Heat Exchanger," *13th Int. Conf. Heat Transf.*

[22] S. Hasebe *et al.*, "Polymer based smart flexible thermopile for power generation," *17th IEEE Int. Conf. Micro Electro Mech. Syst. Maastricht MEMS 2004 Tech. Dig.*, pp. 4–7, 2004.

[23] H. C. Chiu, R. H. Hsieh, Y. J. Chiu, J. H. Jang, and W. C. Lin, "Experimental study on the heat transfer of heat sink with bio-mimetic oscillating foil," *Int. Commun. Heat Mass Transf.*, vol. 68, pp. 130–136, 2015.

[24] P. D. Richardson and K. Tanishita, "Analysis of lowe's measurements of effects of vibration on heat transfer," *Int. J. Heat Mass Transf.*, vol. 17, no. 9, pp. 1118–1119, 1974.

[25] J. B. Lee, S. G. Park, and H. J. Sung, "Heat transfer enhancement by asymmetrically clamped flexible flags in a channel flow," *Int. J. Heat Mass Transf.*, vol. 116, pp. 1003–1015, 2018.

[26] L. Cheng, T. Luan, W. Du, and M. Xu, "Heat transfer enhancement by flow-induced vibration in heat exchangers," *Int. J. Heat Mass Transf.*, vol. 52, no. 3–4, pp. 1053–1057, 2009.

[27] S. G. Park, B. Kim, C. B. Chang, J. Ryu, and H. J. Sung, "Enhancement of heat

transfer by a self-oscillating inverted flag in a Poiseuille channel flow," *Int. J. Heat Mass Transf.*, vol. 96, pp. 362–370, 2016.

[28] F. Selimefendigil, H. F. Öztop, and A. J. Chamkha, "Fluid–structure-magnetic field interaction in a nanofluid filled lid-driven cavity with flexible side wall," *Eur. J. Mech. B/Fluids*, vol. 61, pp. 77–85, 2017.

[29] A. Bar-Cohen, Suzana Prstic, Madhusudan Iyengar, "BYPASS EFFECT IN HIGH PERFORMANCE HEAT SINKS," *Therm. Int. Conf. Sci.*, 2000.

[30] W. S. Fu and W. J. Shieh, "Transient thermal convection in an enclosure induced simultaneously by gravity and vibration," *Int. J. Heat Mass Transf.*, vol. 36, no. 2, pp. 437–452, 1993.

[31] S. Alben, "Improved convection cooling in steady channel flows," *Phys. Rev. Fluids*, vol. 2, no. 10, 2017.

[32] K. Shoele and R. Mittal, "Computational study of flow-induced vibration of a reed in a channel and effect on convective heat transfer," *Phys. Fluids*, vol. 26, no. 12, 2014.

[33] E. Jamesahar, M. Ghalambaz, and A. J. Chamkha, "Fluid-solid interaction in natural convection heat transfer in a square cavity with a perfectly thermal-conductive flexible diagonal partition," *Int. J. Heat Mass Transf.*, vol. 100, pp. 303–319, 2016.

[34] P. Kumar, K. Schmidmayer, F. Topin, and M. Miscevic, "Heat transfer enhancement by dynamic corrugated heat exchanger wall: Numerical study," *J. Phys. Conf. Ser.*, vol. 745, no. 3, pp. 0–8, 2016.

[35] T. Aihara, S. Maruyama, and S. Kobayakawa, "Free convective/radiative heat transfer from pin-fin arrays with a vertical base plate (general representation of heat transfer performance)," *Int. J. Heat Mass Transf.*, vol. 33, no. 6, pp. 1223–1232, 1990.

[36] European Centre for Ecotoxicology and Toxicology of Chemicals, "Linear Polydimethylsiloxanes," *Linear Polydimethylsiloxanes CAS No. 63148-62-9 (second Ed.*, vol. 9, no. 63148, pp. 3–8, 2011.

[37] "Smooth-On, Ecoflex Series," *Prod. Data Sheet*.

[38] "Model : CNB-S1," *ENZOTECH*, p. 1100.

[39] "Thermal Compounds, Adhesives and Interface Materials Product datasheet," *Wakef. Eng.*, pp. 69–73.

[40] G. Medical AG, "Galinstan fluid Safety Data Sheet," pp. 2–5, 2004.

[41] S. C. Agent, "Applying a Silane Coupling," pp. 11–12.

[42] P. G. Pape, "Adhesion Promoters," *Handb. Adhes. Surf. Prep.*, pp. 369–386, 2011.

[43] “Silane Coupling Agents: Connecting Across Boundaries,” *Gelest, Inc.*

[44] J. P. Matinlinna, L. V. J. Lassila, and P. K. Vallittu, “The effect of three silane coupling agents and their blends with a cross-linker silane on bonding a bis-GMA resin to silicatized titanium (a novel silane system),” *J. Dent.*, vol. 34, no. 10, pp. 740–746, 2006.

[45] “(3-TRIMETHOXYSILYLPROPYL)DIETHYLENETRIAMINE, tech-95,” *Gelest Saf. Data Sheet*, vol. 95, pp. 1–8, 2015.

[46] “C11000 ALLOY DATASHEET,” *AJ Oster*, no. 787, p. 11000.

[47] I. H. Bell, J. Wronski, S. Quoilin, and V. Lemort, “Pure and pseudo-pure fluid thermophysical property evaluation and the open-source thermophysical property library coolprop,” *Ind. Eng. Chem. Res.*, vol. 53, no. 6, pp. 2498–2508, 2014.

[48] D. C. Johnson, *Mechanical Vibrations*, vol. 169, no. 4303. 1952.

[49] C. F. Beards and M. Mioa, “Structural Vibration: Analysis and Damping,” *Elsevier*, p. 289, 1996.

[50] M. U. X. Ux, “Specs cameria.”

[51] M. Mohamed and B. Far, “An enhanced threshold based technique for white blood cells nuclei automatic segmentation,” *2012 IEEE 14th Int. Conf. e-Health Networking, Appl. Serv. Heal. 2012*, pp. 202–207, 2012.

[52] S. Gupta and S. Ghosh Mazumdar, “Sobel edge detection algorithm,” *Int. J. Comput. Sci. Manag. Res.*, vol. 2, no. 2, pp. 1578–1583, 2013.

[53] G. B. Reddy, “Implementation of SOBEL Edge Detection on FPGA,” *Int. J. Comput. Trends Technol.*, vol. 3, pp. 472–475, 2016.

[54] Y. Kashyap, A. Vyas, R. Raghuwanshi, and R. Sharma, “Edge Detection Using Sobel Method With Median Filter,” pp. 372–379, 2015.

[55] E. J. Mohammad, M. Jawadkadhim, W. I. Hamad, and S. Y. Helyel, “Study Sobel Edge Detection Effect on the ImageEdges Using MATLAB,” vol. 3, no. 3, pp. 10408–10415, 2014.

[56] K. Gaurav and U. Ghanekar, “Image steganography based on Canny edge detection, dilation operator and hybrid coding,” *J. Inf. Secur. Appl.*, vol. 41, pp. 41–51, 2018.

[57] Y. Meng, Z. Zhang, H. Yin, and T. Ma, “Automatic detection of particle size distribution by image analysis based on local adaptive canny edge detection and modified circular Hough transform,” *Micron*, vol. 106, no. August 2017, pp. 34–41, 2018.

[58] J. Lei, F. Lee Wang, H. Deng, and D. Miao, *LNAI 7530 - Artificial Intelligence and Computational Intelligence*. .

[59] M. Mohamed and G. Alaghband, “An Improved Parallel Eight Direction Prewitt Edge Detection Algorithm.”

[60] K. Lakhani, B. Minocha, and N. Gugnani, “Analyzing edge detection techniques for feature extraction in dental radiographs,” *Perspect. Sci.*, vol. 8, pp. 395–398, 2016.

[61] X. Yuan, W. Gao, and H. Zhang, “A new algorithm of image filtering based on matlab,” *2012 Spring World Congr. Eng. Technol. SCET 2012 - Proc.*, no. 51005071, pp. 1–4, 2012.

[62] D. J. Inman, *Vibration with Control*. 2006.

[63] A. Sinha, *Vibration of mechanical systems*, vol. 3, no. September. Cambridge University Press, 1981.

[64] B. Balachandran and E. Magrab, *Vibrations*. Cengage Learning, 2009.

[65] M. J. Maurizi, R. E. Rossi, and J. A. Reyes, “Vibration frequencies for a uniform beam with one end spring hinged and subjected to a translational restraint at the other end,” *J. Sound Vib.*, vol. 48(4), pp. 565–568, 1976.

[66] K. R. Chun, “Free Vibration of a Beam With One End Spring-Hinged and the Other Free,” *J. Appl. Mech.*, vol. 39, no. 4, p. 1154, 2010.

[67] Z. Y. Zhong, J. P. Zhou, H. L. Zhang, and T. Zhang, “Effect of the equivalent stiffness of flexible supports on the MEMS cantilever-based sensors,” *Comput. Struct.*, vol. 169, pp. 101–111, 2016.

[68] F. P. INCROPERA, D. P. DEWITT, T. L. BERGMAN, and A. S. LAVINE, *Fundamentals of Heat and Mass Trasfer*, no. 1986. 1993.

[69] Y. A. Cengel and A. J. Ghajar, *Heat and Mass Transfer: Fundamentals and Applications*. McGraw-Hill Education, 2015.

[70] Y. Joo and S. J. Kim, “Comparison of thermal performance between plate-fin and pin-fin heat sinks in natural convection,” *Int. J. Heat Mass Transf.*, vol. 83, pp. 345–356, 2015.